Microelectronic Engineering 299 (2025) 112364

Contents lists available at ScienceDirect

Microelectronic Engineering

journal homepage: www.elsevier.com/locate/mee

Research paper

Assessing the performance of perovskite solar cells under Peltier cooling

A. Kaltzoglou [a,*], E. Christopoulos [a,b], D.N. Kossyvakis [a,c], N.S. Tagiara [a], P. Falaras [b], N.K. Nasikas [b,d], E.V. Hristoforou [e], M.M. Elsenety [b,f]

[a] Theoretical and Physical Chemistry Institute, National Hellenic Research Foundation, 11635 Athens, Greece
[b] Institute of Nanoscience and Nanotechnology, National Center for Scientific Research "Demokritos", 15310, Agia Paraskevi Attikis, Athens, Greece
[c] School of Mining and Metallurgical Engineering, National Technical University of Athens, 15780 Zografou, Athens, Greece
[d] Department of Military Studies, Division of Mathematics and Engineering Sciences, Hellenic Army Academy, 16673, Vari, Attica, Greece
[e] School of Electrical and Computer Engineering, National Technical University of Athens, 15780 Zografou, Athens, Greece
[f] Department of Chemistry, Al-Azhar University, P.O. 11823, Nasr City, Cairo, Egypt

ARTICLE INFO

Keywords:
Halide perovskites
Peltier cooling
Hybrid devices
Heat-transfer simulations
Thermoelectric materials

ABSTRACT

The commercialization of perovskite solar cells (PSCs) has been restricted so far due to their short life time, which is partly attributed to their instability at high operating temperatures. The current paper studies the performance of the cells under Peltier cooling. The experimental setup includes a perovskite solar cell and a Peltier cooler beneath, where the latter is connected to an external power supply. The temperature on the surface of the solar cell spans over the range ca. 5 °C to 50 °C under 1 sun illumination, depending on the power input of the Peltier cooler. The *J-V* measurements indicate a non-linear temperature dependence of the power conversion efficiency (PCE), which reaches a maximum of 18.1 % at 27 °C, whereas at temperatures close to 50 °C the PCE drops significantly. The experimental results are combined with more generic theoretical simulations for scaling up the PSC unit, which provides electrical power to the Peltier unit. The simulations examine the ability of different system configurations to maintain the solar cell temperature below 50 °C without significant deterioration of the electrical performance of the hybrid PSC – Peltier device. Overall, the results show that a large-scale PSC – Peltier device is feasible for both roof-integrated and rooftop installation types, in order to protect the solar cell from overheating and degradation.

1. Introduction

Despite that the PCE of PSCs currently exceeds 25 % [1], their instability for long-term use in ambient conditions remains unsolved [2]. Many researchers focus on the effect of elevated temperatures on performance of PSCs [3–9], One approach to resolve their overheating issue is via the thermoelectric effect. This, in principle, splits into two directions: a) the Seebeck effect, where a thermoelectric material beneath the solar cell dissipates heat, thus reducing the solar cell temperature and generating electricity from wasted heat and b) the Peltier effect, where an external electric current is applied to the thermoelectric module to cool down the solar cell. The first approach of photovoltaic – thermoelectric generator (PV – TEG) for combined electrical energy conversion from light and heat, respectively [10–16] has been well studied not just for PSCs but also for silicon-based photovoltaics. It results in moderate heat dissipation from the solar cell to the thermoelectric unit and low energy efficiency of the latter compared to the solar cell. The second approach of utilizing thermoelectric cooling (TEC) (also known as Peltier cooling) for active thermal management of photovoltaic modules (and in particular PSCs that are much more sensitive to high temperatures than silicon-based solar cells) has been recently investigated. Theoretical simulations have proved that the operation of PV-TEC hybrid systems is viable [17–19] as it may drop significantly the operating temperature of the solar cell. To our knowledge, their PSC-TEC counterparts have not been experimentally studied so far.

In this work, the performance of a small-scale hybrid PSC-TEC system is experimentally evaluated under different temperatures. The findings of this innovative process are then used to identify optimum operating configurations for large-scale PSC-TEC hybrids through an analytical modeling approach for a given set of ambient conditions.

* Corresponding author.
E-mail address: akaltzoglou@eie.gr (A. Kaltzoglou).

https://doi.org/10.1016/j.mee.2025.112364
Received 16 March 2025; Received in revised form 13 May 2025; Accepted 25 May 2025
Available online 27 May 2025

2. Materials and methods

2.1. Perovskite solar cell fabrication

The reagents titanium diisopropoxide, lead iodide (PbI_2), lead bromide ($PbBr_2$), methylammonium bromide (MABr), formamidinium iodide (FAI), dimethylformamide (DMF), dimethyl sulfoxide (DMSO), acetonitrile, anhydrous ethanol (EtOH), anhydrous chlorobenzene and 4-tert-butylpyridine (TBP), were obtained from Sigma-Aldrich. Lithium bis(trifluoromethylsulphonyl)imide (Li-TFSI) was purchased from Acros, tris(2-(1H-pyrazol-1-yl)-4-tert-butylpyridine)-cobalt(III)-tris(bis (trifluoromethylsulfonyl)imide)) FK209 from Sigma-Aldrich and TiO_2 18NRT paste from Dyesol. Fluorine-doped tin oxide (FTO) transparent and conductive glass electrodes (7 Ω/sq) were cleaned in ultrasounds with Hellmanex III, deionized water, acetone, and isopropanol for 15 min each step and dried using N_2 flow. Then the cleaned glasses were treated with UV-ozone for 20 min. On the FTO electrodes, the TiO_2 blocking layer was spin-coated at 4000 rpm for 30 s and sintered at 450 °C for 30 min. The mesoporous TiO_2 layer was deposited by spin-coating 6000 rpm for 30 s of a precursor solution of 150 mg TiO_2 paste diluted in EtOH (1:12 *w*/w). The substrates were immediately dried at 125 °C for 5 min, and then sintered at 325 °C, 375 °C, 450 °C for 5 min, 5 min and 30 min, respectively. The triple perovskite film of the nominal composition $Cs_{0.08}(FA_{0.83}MA_{0.17})_{0.92}Pb(I_{0.9}Br_{0.1})_3$ was deposited in an Ar-filled glovebox by spin-coating upon the TiO_2 substrates. The perovskite precursor solution was prepared using 1.1 mol L^{-1} PbI_2, 0.2 mol L^{-1} $PbBr_2$, 1 mol L^{-1} FAI and 0.2 mol L^{-1} MABr in 850 μL of mixed DMSO: DMF (1: 4 volume ratio) solvent. 42.5 μL of 2 mol L^{-1} CsI in DMSO were added to the perovskite solution. The combined solution was spin-coated in two steps at 1000 rpm for 10 s and, then at 6000 rpm for 20 s. For an antisolvent treatment, 5 s before the end of the second step, 150 μL of anhydrous chlorobenzene were poured on the film which was post-annealed at 100 °C for 60 min. After cooling down to room temperature, 2,2′,7,7′-tetrakis(*N*,*N*-di-p-methoxyphenylamine)-9,9′-spirobifluorene (spiroMeOTAD) was spin-coated at 4000 rpm for 15 s. This solution was prepared by dissolving 73.5 mg of Spiro-OMeTAD in 1 mL of anhydrous chlorobenzene, then adding 29 μL of tert-butyl pyridine (tBP), 17 μL of Li-TFSI salt (540 mg/1 mL acetonitrile), and 8 μL of FK209 (375.8 mg/1 mL acetonitrile). At the end, counter electrodes of 100 nm thick Ag were thermally evaporated. Overall, the devices (Fig. 1a) consisted of FTO/ compact TiO_2 (c-TiO_2)/ mesoporous TiO_2 (m-TiO_2)/ (FA/MA/Cs)$PbI_{3-x}Br_x$ /Spiro-MeOTAD /Ag layers. TiO_2 and Spiro-MeOTAD act as the electron and hole transporting layers, respectively. Current density - voltage (*J-V*) characteristics were obtained under 1 sun illumination conditions (A.M. 1.5G) with an Autolab potentiostat (PGSTAT-302 N) at a scan rate of 150 mV sec^{-1} with active (illuminated) area of 0.097 cm^2.

2.2. Peltier module and heat exchange with the perovskite solar cell

For the purpose of the Peltier cooling, a Wakefield-Vette TEMA-AP-40-12 Thermoelectric Assembly (Direct-Air to Plate, 12 VDC, 40 W, 3.9 A, 120 × 102 × 80 mm unit) [20] was used (Fig. 1b). A custom-made aluminum-tin plate was screwed to its surface in order to achieve direct contact and therefore high heat transfer to the PSC unit that sat directly on the plate with an interface of ca. 5 × 15 mm. The Peltier cooler was powered by a TTi CPX400D unit, whose output was manually adjusted from 0 W (no cooling) to 40 W (maximum cooling). The temperature on the top surface of the perovskite solar cell inside the Ossila platform (Fig. 1c) was monitored via a Flir One thermal camera. The area around the PV-TE system was purged with argon throughout the experiment in order to avoid the condensation of ice on the solar cell under intensive Peltier cooling. For reference, the surface of the Peltier module, when free, reaches ca. -15 °C at maximum power input. In contrast, the surface of the PSC in the Ossila platform and on the Peltier cooler reaches temperatures of ca. 3 °C (Fig. 1d), under maximum output power, due to the inevitable heat losses. It is also worth mentioning that other Peltier modules of smaller size (e.g. 5 × 5 mm) could be attached directly via thermal paste to the PSC, but they did not provide adequate cooling of the latter even with high input power.

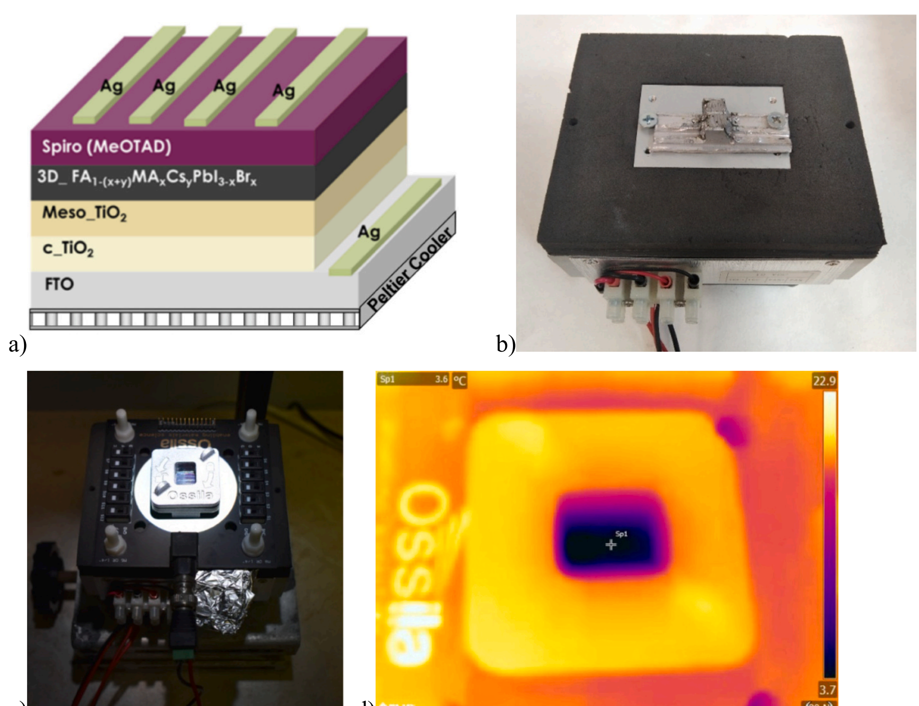

Fig. 1. a) Architecture of the PSC and the Peltier cooler underneath it, b) photograph of the Peltier cooler with modified surface for efficient heat exchange with the PSC, c) photograph of the full experimental setup of the Peltier cooler and the PSC on the Ossila platform under 1 sun illumination, d) thermal camera image of the PSC and the Peltier cooler at maximum input power. The value on the cross refers to the temperature on the solar cell surface in the dark, namely 3.6 °C.

2.3. Theoretical simulations

2.3.1. Analytical model

For the purpose of assessing the performance of the proposed hybrid system, an analytical modeling approach has been employed. The model describes the steady-state energy balance established for a PSC module with TECs incorporated on the back (not limited to partial cover of the PSC surface as in the small-scale experimental setup above), taking into account the electrical parameters of interest as well as all incoming and outgoing heat flux mechanisms (module's power output, TEC power consumption, solar irradiance input, heat transfer through inner layers, radiation and convection heat exchange between the system and the environment). Calculation of the main electrical performance parameters and the temperature established in the different layers of the hybrid structure becomes possible in this manner (details on the mathematical formulation can be found in [17] and [21]). In principle, the model is identical to simulation approaches previously developed for the case of conventional PV module installations [22]. Nevertheless, an additional term must be accounted for the energy balance established between the PSC backside and the environment, in order for the cooling effect induced by the thermoelectric subsystem to be considered (see Supporting Information).

2.3.2. PV installation types

Naturally, when examining the hybridization of TEC devices and PSCs (or any PV cell type in general), the main focus is on the installation types operating under elevated temperatures. Apart from the ambient conditions, the other critical factor to define cell temperature is the type of installation, as it greatly affects the ability of the system to effectively exchange heat with the environment [23]. A rational classification of the various types of PV installations according to their operating temperature is provided in [24], distinguishing between four different groups. Despite that the particular classification refers to crystalline Si-based solar cells, extending its applicability to other PV technologies (including PSCs) can be justified. The electrical efficiency, which defines the internally generated heat available to raise the temperature of each cell, differs through the various cell types. The heat exchange mechanisms acting on any PV module, however, can be considered identical, if all installation-related parameters are equal.

In this respect, the two PSC-TEC hybrid groups of main interest would be roof-integrated and rooftop installations with limited distance (< 10 cm) between the module and the building block beneath. In this case, heat exchange between the module and the environment becomes inherently more restricted, resulting in elevated operating temperatures. In more detail, operating temperatures approaching 80 °C and 60 °C should be expected for the case of stand-alone PSCs for the particular two groups for the same ambient conditions as assumed here [17]. Having in mind the 50 °C threshold identified through the experimental process for the PSC that undergoes an efficiency drop or even an irreversible decomposition, the reasoning behind focusing the theoretical assessment to those particular installations classes becomes evident.

2.3.3. PSC parameters

The aim of this study is to simulate as closely as possible the actual performance of a PSC module in stand-alone as well as hybrid mode. To investigate the performance of the tandem PSC-TEC hybrid via the proposed modeling approach, various parameters relevant to the electrical efficiency as well as the structural characteristics of the perovskite module have to be inserted into the analytical model. It must be kept in mind, however, that the commercialization status of PSCs is currently at an early stage. While a reasonable amount of data on their electrical performance can be found in the relevant literature [3], not all the information relevant to the construction of an actual PSC module is currently readily available. Inevitably, certain assumptions had to be made on the basis of the most recent advancements in the field of perovskite solar cells technology. The main performance and construction parameters of the PSC necessary to develop the simulation process are summarized in Table S1, along with references for the values.

2.3.4. Peltier parameters

With regard to the Peltier cooler and for the purposes of the simulation process, Bi_2Te_3-based thermoelectric coolers have been considered. Bi_2Te_3 exhibits superior thermoelectric performance for operating conditions ranging from room temperature up to approximately 200 °C [25]. Taking into account the temperature ranges involved, the material of choice becomes well justified. Regarding the geometrical parameters, the TEC device is assumed to include 127 TE legs with cross section equal to 1.0×1.0 mm^2. Since previous studies on PV-TEC hybrids indicated improved overall performance for TEC units of shorter leg length [17], this parameter has been set to 13 mm, which corresponds to the lower end of leg lengths commonly addressed in commercially available devices.

When it comes to the individual properties of the *p*- and *n*-type semiconducting materials assumed for the construction of the leg, temperature-dependent properties have been assigned. Publicly available information provided by manufacturers of thermoelectric coolers have been taken into account for this purpose [26]. Seebeck coefficient, thermal conductivity and electrical conductivity parameters for the *p*- and *n*- semiconducting materials respectively are provided in the form of the coefficients of their 2nd order polynomial expressions in Table S2. The calculated dimensionless thermoelectric figure of merit ZT at room temperature for the below stated parameters equals 0.88 and 0.84 for the *p*- and *n*-type materials respectively. These values are within the range expected for commercially available thermoelectric materials, such as Bi_2Te_3 [25].

To identify optimal configurations, a sensitivity study has been performed by varying the number of thermoelectric coolers attached on the back of the PSC (N_{TEC}) within the range of 15–75 TECs/m^2 and the voltage input fed to each individual TEC (V_{TEC}) between 0.1 V and 1.0 V. One additional parameter affecting the performance of the system refers to the heat exchange conditions on the hot side of the TEC, where heat is released to the ambient environment. A fin-type air cooled heat sink of constant thermal resistance equal to 2 K/W has been assumed for the purposes of the simulation process. The assumed value is in good agreement to the range of the thermal resistances provided by heat sink manufacturers for fin type air cooled heat sinks under natural convection mode and having size similar to the thermoelectric units considered here [27].

2.3.5. Ambient parameters

With regard to ambient conditions and the heat exchange mechanisms assumed, since steady-state performance is of interest, constant values have been regarded for both solar irradiance and ambient temperature inputs to the model (1000 W/m^2 and 30 °C respectively). The main heat exchange mechanisms to be considered refer to radiation and convection for both the frontal and the backsheet area of the PSC module. For the module frontal, emissivity has been set in accordance to values commonly addressed in the literature for transparent glass (see Table S2). For the module backsheet, radiation heat exchange has been completely neglected, assuming rear module temperature approximately equal to the temperature of the building element beneath. This approach is reasonable for the installation types examined here due to the relatively small distance between the module and the building's roof [28].

The definition of the convection coefficients has been developed in a different manner, partially distinguishing between the two installation types examined. For module frontal area, the same formula (as proposed in [29]) has been used to define convection coefficient (h_{cf}) for both roof-integrated and rooftop classes:

$$h_{cf} = 2.8 + 3.0V_w$$

 Microelectronic Engineering 299 (2025) 112364

where V_w stands for the wind speed and also depends on the type of installation. For the purposes of the simulation process executed here, V_w has been set equal to 0.5 m/s and 1.2 m/s for roof-integrated and rooftop systems respectively, which is in agreement to the findings of [30]. The same formula has been used to define convection coefficient for module rear (h_{cb}) when considering rooftop installations. On the other hand, a constant coefficient equal to 0.5 W m^{-2} K^{-1} has been assumed for the case of roof-integrated installations [31].

3. Results and discussion

3.1. Effect of temperature on perovskite solar cell performance

PSCs exhibit temperature-dependent behavior that significantly influences their photovoltaic performance, including short-circuit current density (J_{sc}), open-circuit voltage (V_{oc}), fill factor (FF), the current density at maximum power (J_{mpp}), voltage at maximum power (V_{mpp}) and overall PCE. Table 1 and Fig. 2 present the performance metrics of PSCs under different operating temperatures ranging from 45 °C (no cooling) to 18 °C (maximum cooling), allowing for an analysis of photothermal effects on device efficiency. The temperatures refer to the values recorded by the thermal camera, immediately after the completion of the J-V measurement. The results indicate that J_{sc} increases with rising temperature up to 24.356 mA/cm^2, compared to 20.371 mA/cm^2 at low temperatures. This trend is attributed to enhanced carrier generation and increased charge carrier mobility at elevated temperatures. However, V_{oc} exhibits an inverse relationship with temperature, decreasing from 1.078 V at 18 °C to 0.967 V at 45 °C. A similar trend was also observed for J_{mpp} and V_{mpp}. This decline is primarily due to an increase in recombination rates and a reduction in the built-in potential of the cell, which weakens the driving force for charge separation.

However, PCE shows a non-linear temperature dependence, with a maximum of 18.16 % at 27 °C and decreasing at both higher (15.79 % at 45 °C) and lower (16.07 % at 18 °C) temperatures. This behavior suggests that moderate operating temperatures optimize carrier transport and reduce resistive losses. In contrast, excessive heating accelerates degradation mechanisms such as ion migration and phase instability in the perovskite layer. A similar behavior was observed in the reported thermal stability of mesoporous triple-cation PSCs over a wide temperature range (−5 °C to 80 °C), demonstrating that elevated temperatures induce irreversible performance losses, primarily due to the evaporation of additives in the hole extraction layers (HELs) and increased recombination rates [3]. This finding further confirms the inverse relationship between temperature and open-circuit voltage (V_{oc}), as observed in our study. Additionally, both studies show that while short-circuit current density (J_{sc}) tends to increase with temperature due to enhanced carrier mobility, the overall PCE exhibits a non-linear trend, peaking at an optimal temperature before declining at higher temperatures, due to increased resistive losses and degradation mechanisms. These effects highlight the critical role of thermal management strategies in maintaining PSC stability and efficiency under real-world operating conditions.

In addition, the correlation matrix provides insights into how temperature affects the photovoltaic parameters and resistances in perovskite solar cells as shown in Fig. 2b. A strong negative correlation (−0.98) indicates that as temperature increases, V_{oc} and FF significantly decrease. This is expected, as higher temperatures increase recombination losses, and reduce the built-in potential, thereby lowering V_{oc} and FF as well. In contrast, J_{sc} increases with increasing temperature. This suggests that higher temperatures enhance charge-carrier generation and mobility, likely due to increased thermal energy aiding carrier transport and a decline in overall performance. Overall, these findings underscore the importance of thermal management strategies, such as passive or active cooling techniques, to stabilize PSC efficiency and longevity in real-world applications. Moreover, it proves higher sensitivity of PSCs compared to Si-based and dye-sensitized solar cells which exhibit a reversible drop in PCE above 40 °C due to the increased recombination rates [32].

Table 1
PSC efficiency at various temperatures.

T (°C)	J_{sc} (mA/cm^2)	V_{oc} (V)	FF	PCE (%)	J_{mpp} (mA/cm^2)	V_{mpp} (V)
45	22.958	0.967	0.711	15.786	20.893	0.756
36	24.356	1.011	0.717	17.656	22.070	0.800
27	23.325	1.067	0.730	18.161	21.227	0.856
18	20.371	1.078	0.732	16.065	18.536	0.867

3.2. Theoretical simulations

In the following sections, the results of the performance assessment of the PSC-TEC hybrid system are presented. The overall aim of this investigation would be to identify configurations able to maintain the temperature of the cells below the threshold of 50 °C identified through the experimental process. At the same time, it is equally important for any proposed hybrid configuration to achieve the required operating temperature without any deterioration in electrical performance. For this reason, the analysis provided below is primarily focused on both of these aspects. To distinguish between the two installation cases considered here (roof-integrated and rooftop with restricted distance between module and roof element), the results are provided for each case separately.

3.2.1. Roof-integrated installations

An illustration of PSC temperature variation vs. the number of TEC units employed per m^2 (N_{TEC}) as well as the voltage fed to each TEC (V_{TEC}) is provided below. The resulting temperature of the cells is plotted for two selected values of V_{TEC} and N_{TEC} respectively. It should be noted that for the case of roof-integrated stand-alone PSC (without TEC integration on the back side) the operating temperature of the perovskite cell reaches 77.8 °C.

As expected, the temperature of the cells decreases while more TEC units are attached and more power is fed to the TEC array by raising the voltage input V_{TEC}. Increasing N_{TEC} or/and V_{TEC} parameters enhances the cooling effect induced by the TEC subsystem, naturally resulting in further reduction of the operating temperature of the PSCs.

It can be observed, however, that not all hybrid configurations examined are able to maintain the temperature of the cells below 50 °C. Fig. 3a reveals that the operating temperature is sufficiently reduced only for the upper limit of N_{TEC} examined here (75 TECs/m^2). The importance of increasing the size of the TEC array is also highlighted by the results of Fig. 3b, where again reduction below the 50 °C threshold can be achieved only for N_{TEC} equal to 75 TECs/m^2. This is, however, a quite remarkable temperature reduction when compared to the case of a stand-alone PSC. Even for the minimum value of V_{TEC} examined for the purposes of this study (0.1 V), the temperature reduction achieved exceeds 29 °C for roof-integrated installations (77.8 °C for the stand-alone PSC vs. 48.6 °C for the PSC-TEC hybrid), assuming N_{TEC} equal to 75 TECs/m^2.

While the outcome of employing a TEC array of increased size in order to reduce operating temperature is straightforward, the optimization process should also address the optimum operating point in terms of the voltage input V_{TEC} fed to each TEC unit. Fig. S1 highlights that TEC power consumption P_{TEC} exponentially increases while raising V_{TEC}. While any increase in V_{TEC} would obviously enhance the cooling effect induced, it could compromise at the same time the electrical performance of the system. As mentioned before, the critical parameter to provide insight on the electrical performance of the system is hybridization power output gain ΔP. The hybridization concept becomes favorable only as long as ΔP remains positive.

To obtain a clearer view on this aspect, in Fig. 4 the variation in ΔP

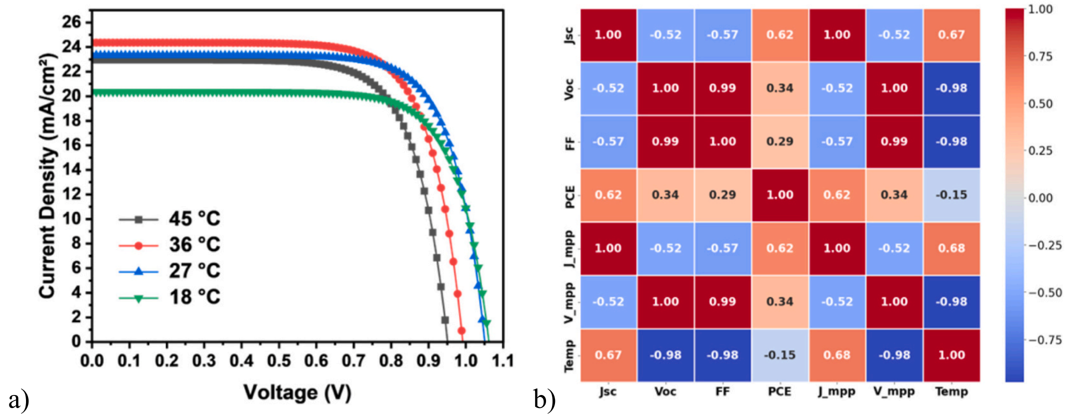

Fig. 2. a) J-V curves of PSCs at various temperatures, b) Heatmap of the correlation matrix of temperature and photovoltaic parameters.

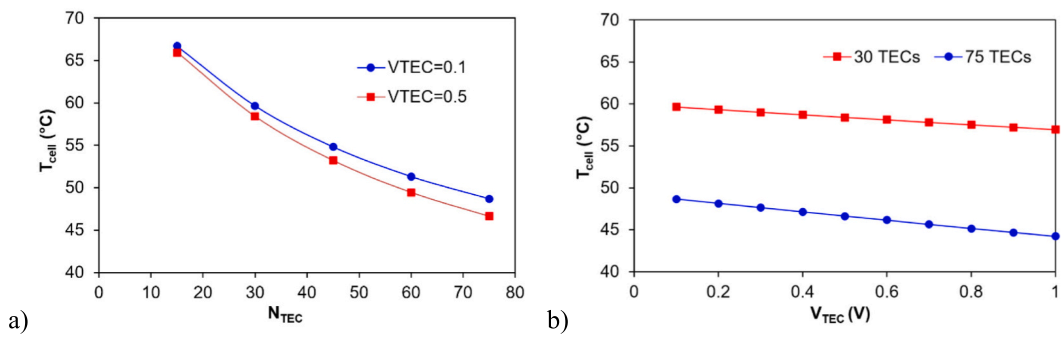

Fig. 3. PSC temperature vs. N_{TEC} (a) and V_{TEC} (b) for roof-integrated installations.

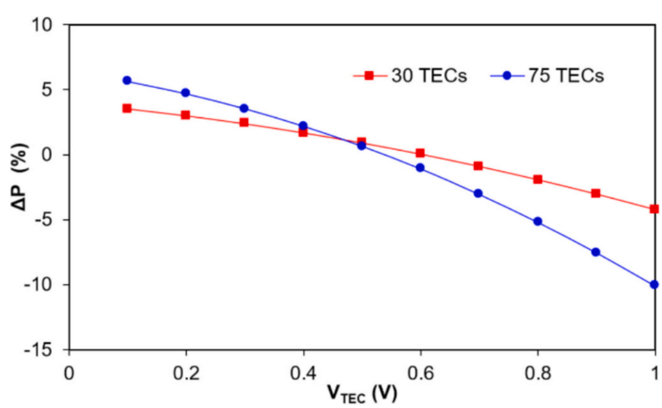

Fig. 4. Hybridization power output gain ΔP vs. V_{TEC} for roof-integrated installations.

while varying parameter V_{TEC} is illustrated for two different settings of N_{TEC} (30 and 75 TECs/m^2, respectively). It can be observed that for both settings, hybridization would prove favorable only for lower values of V_{TEC}. A threshold can also be identified above which ΔP becomes negative. This threshold, however, clearly depends on the N_{TEC} parameter. It is interesting to note that the overall optimum operating point is achieved for the lowest value of V_{TEC} examined (0.1 V).

Having in mind the results of this analysis, it can be concluded that for roof-integrated PSC-TEC hybrids, an optimal configuration would dictate the utilization of a large TEC array operating under a low power consumption mode. Although feeding more power to the TECs would result in decreased operating temperature for the cells, Fig. S2 indicates that this would come at the expense of the system's overall electrical performance. Taking also into account the results of Fig. 2, it should be highlighted that a temperature reduction of more than 29 °C (bringing the cell below the detrimental limit 50 °C) becomes possible, while still achieving improved electrical performance for the hybrid system vs. a stand-alone PSC (ΔP reaches a maximum of 5.6 %).

3.2.2. *Rooftop installations*

In Fig. 5, the resulting temperature of the cells coming from the sensitivity analysis is plotted for selected values of V_{TEC} and N_{TEC} for the case of rooftop PSC-TEC hybrids. It should be noted that for the particular installation case the temperature of the perovskite cell reaches 59.1 °C when in stand-alone mode.

The temperature of the cells decreases again while increasing parameters N_{TEC} and V_{TEC} due to the enhanced cooling effect introduced. In this case, however, it can be observed that even TEC arrays of smaller size would be able to achieve operating temperatures below 50 °C. This should be attributed to the lower operating temperature of the rooftop stand-alone PSC when compared to the roof-integrated case. As the stand-alone cell operates at 59.1 °C, any reduction of more than 9 °C would be considered sufficient to avoid irreversible decomposition. For the same reason, however, the cooling effect cannot be as effective for rooftop systems as for roof-integrated hybrids. For the lowest V_{TEC} value of 0.1 V, the resulting temperature reduction reaches 7.9 °C and 14 °C for N_{TEC} equal to 30 and 75 TECs/m^2 respectively. While obviously it is still possible to maintain the temperature of the cell below the limit of 50 °C, the temperature reduction achieved is well below the improvement identified for roof-integrated systems.

When it comes to the optimal operating point in terms of V_{TEC} setting, Fig. S2 indicates that similar considerations as for the case of roof-integrated hybrids should apply. P_{TEC} again demonstrates an exponential increase while raising V_{TEC}, indicating that an optimum operating point should exist. In Fig. 6 the variation in ΔP vs. V_{TEC} is plotted for two different values of N_{TEC} (30 and 75 TECs/m^2

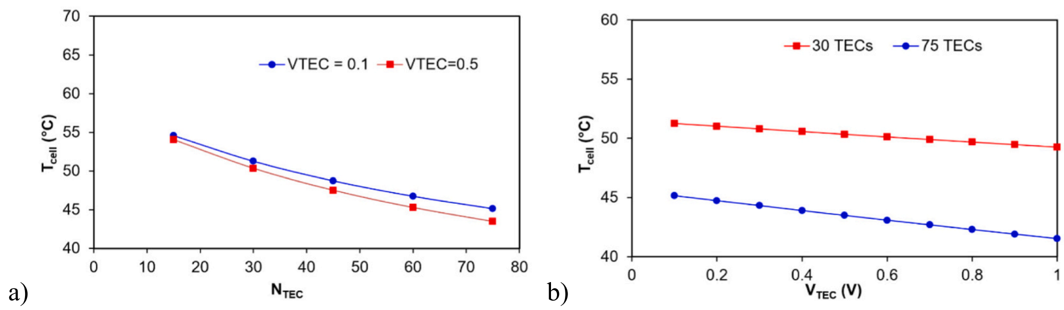

Fig. 5. PSC temperature vs. N_{TEC} (a) and V_{TEC} (b) for rooftop installations.

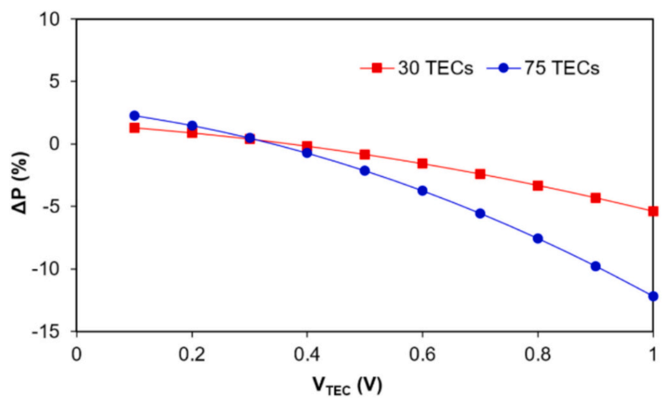

Fig. 6. Hybridization power output gain ΔP vs. V_{TEC} for rooftop installations.

respectively). Although the maximum improvement in power output is obviously restricted for rooftop PSC-TEC hybrids reaching 2.3 %, the trend identified is very similar to the case of roof-integrated systems. Lower values of V_{TEC} provide improved overall electrical performance, while any improvement is practically eliminated for V_{TEC} exceeding 0.3 V.

It can be therefore concluded that an optimal configuration for rooftop PSC-TEC hybrids would also foresee the employment of a TEC array of increased size operating under a low power consumption mode. Even though the improvement achieved does not reach the levels addressed for roof-integrated systems, the stand-alone rooftop PSC also exceeds the 50 °C limit for the set of ambient conditions examined here. Planning for some means of cooling mechanism becomes, in this sense, important also for the case of rooftop PSC installations, at least when the system is installed in areas of increased levels of solar irradiance and where high ambient temperatures are common for an extensive period of time through the year.

4. Conclusions

In this work, the characteristics of a hybrid PSC-TEC system have been evaluated. The experimental setup based on an externally-powered TEC indicate that the PCE of the PSCs varies with the temperature and it drops significantly over 50 °C. In contrast to the experimental setup where the power consumption of the TEC is much larger than the power output of the PSC, the theoretical simulations involve a self-powered system, where the power on the TEC is supplied by the PSC unit. This seems appealing for large-scale systems, and it offers an alternative to passive cooling mechanisms for PV devices. The balance between power output and efficient cooling of the solar cells depends largely on the sensitivity of the latter to high temperatures. These findings of our simulations could prove useful for the industrilization of perovskite solar cells by taking into account their thermal management constraints and the available cooling mechanisms.

CRediT authorship contribution statement

A. Kaltzoglou: Writing – review & editing, Funding acquisition, Project administration. **E. Christopoulos:** Methodology, Investigation, Validation. **D.N. Kossyvakis:** Methodology, Investigation, Validation. **N.S. Tagiara:** Methodology, Investigation, Validation. **P. Falaras:** Writing – review & editing. **N.K. Nasikas:** Methodology, Investigation, Validation. **E.V. Hristoforou:** Writing – review & editing. **M.M. Elsenety:** Methodology, Investigation, Validation.

Declaration of competing interest

The authors declare that they have no known competing financial interests or personal relationships that could have appeared to influence the work reported in this paper.

Acknowledgements

The research project was supported by the Hellenic Foundation for Research and Innovation (H.F.R.I.) under the “2nd Call for H.F.R.I. Research Projects to support Post-Doctoral Researchers” (Project Number: 450).

Appendix A. Supplementary data

Supplementary data to this article can be found online at https://doi.org/10.1016/j.mee.2025.112364.

Data availability

Data will be made available on request.

References

[1] https://www.nrel.gov/pv/cell-efficiency.html.
[2] A. Julien, J.-B. Puel, J.-F. Guillemoles, Distinction of mechanisms causing experimental degradation of perovskite solar cells by simulating associated pathways, Energy Environ. Sci. 16 (2023) 190–200, https://doi.org/10.1039/D2EE03377A.
[3] I. Mesquita, L. Andrade, A. Mendes, Temperature impact on perovskite solar cells under operation, ChemSusChem 12 (2019) 2186–2194, https://doi.org/10.1002/cssc.201802899.
[4] T.J. Jacobsson, W. Tress, J.-P. Correa-Baena, T. Edvinsson, A. Hagfeldt, Room temperature as a goldilocks environment for $CH_3NH_3PbI_3$ perovskite solar cells: the importance of temperature on device performance, J. Phys. Chem. C 120 (2016) 11382–11393, https://doi.org/10.1021/acs.jpcc.6b02858.
[5] Q. Meng, Y. Chen, Y.Y. Xiao, J. Sun, X. Zhang, C.B. Han, H. Gao, Y. Zhang, H. Yan, Effect of temperature on the performance of perovskite solar cells, J. Mater. Sci. Mater. Electron. 32 (2021) 12784–12792, https://doi.org/10.1007/s10854-020-03029-y.
[6] W. Tress, K. Domanski, B. Carlsen, A. Agarwalla, E.A. Alharbi, M. Graetzel, A. Hagfeldt, Performance of perovskite solar cells under simulated temperature-illumination real-world operating conditions, Nat. Energy 568 (2019) 568–574, https://doi.org/10.1038/s41560-019-0400-8.
[7] L. Lin, N.M. Ravindra, Temperature dependence of CIGS and perovskite solar cell performance: an overview, Appl. Sci. 2 (2020) 1361, https://doi.org/10.1007/s42452-020-3169-2.

[8] J. Liu, Y. Zhou, Z. Zhou, Y. Du, C. Wang, X. Yang, Z. Lin, Z. Guo, J. Zhao, L. Ye, H. Zhang, J. Yan, Passive photovoltaic cooling: advances toward low-temperature operation, Adv. Energy Mater. 14 (2024) 2302662, https://doi.org/10.1002/aenm.202302662.
[9] T. Ma, Y. An, Z. Yang, Z. Ai, Y. Zhang, C. Wang, X. Li, Thermodynamic processes of perovskite photovoltaic, devices: mechanisms, simulation, and manipulation, Adv. Funct. Mater. 33 (2023) 2212596, https://doi.org/10.1002/adfm.202212596.
[10] J. Zhang, Y. Xuan, L. Yang, A novel choice for the photovoltaic-thermoelectric hybrid system: the perovskite solar cell, Int. J. Energy Res. 40 (2016) 1400–1409, https://doi.org/10.1002/er.3532.
[11] Y. Zhou, Y. Chen, Q. Zhang, Y. Zhou, M. Tai, K. Koumoto, H. Lin, A highly-efficient concentrated perovskite solar cell-thermoelectric generator tandem system, J. Energy Chem. 59 (2021) 730–735, https://doi.org/10.1016/j.jechem.2020.12.020.
[12] B. Lorenzi, P. Mariani, A. Reale, A. Di Carlo, G. Chen, D. Narducci, Practical development of efficient thermoelectric – photovoltaic hybrid systems based on wide-gap solar cells, Appl. Energy 300 (2021) 117343, https://doi.org/10.1016/j.apenergy.2021.117343.
[13] S. Oh, P. Rai, M. Ramasamy, V.K. Varadan, Fishnet metastructure for IR band trapping for enhancement of photovoltaic–thermoelectric hybrid systems, Microelectron. Eng. 148 (2015) 117–121, https://doi.org/10.1016/j.mee.2015.10.016.
[14] Y. Hu, P. Li, Y. Yao, H. Lv, C. Xu, Numerical analysis and performance investigation of holographic spectrum-splitting concentrated photovoltaic-thermoelectric hybrid system with phase change material, Energy Convers. Manag. 328 (2025) 119571, https://doi.org/10.1016/j.enconman.2025.119571.
[15] W. Tian, X. Zheng, Y. Xiao, G. Qin, A novel photovoltaic-thermoelectric hybrid system with an anisotropic shape-stale phase change composites, J. Energy Storage 104 (2024) 114676, https://doi.org/10.1016/j.est.2024.114676.
[16] P. Lai, X. Han, X. Chen, J. Huang, All-day continuous power generation: integrating radiative cooling with semi-transparent photovoltaic cells filtered concentrated photovoltaic-thermoelectric generator system, Sol. Energy 287 (2025) 113207, https://doi.org/10.1016/j.solener.2024.113207.
[17] D.N. Kossyvakis, E.V. Christoforou, P. Falaras, A. Kaltzoglou, Optimum coupling of photovoltaic devices and Peltier coolers for improved performance and stability, Int. J. Sustain. Energy 41 (2022) 1667–1693, https://doi.org/10.1080/14786451.2022.2092481.
[18] R. Hamzehzarghani, M. Eslami, Feasibility evaluation of a thermoelectrically cooled photovoltaic module at different arrangements and working conditions: A numerical study, Therm. Sci. Eng. Prog. 48 (2024) 102382, https://doi.org/10.1016/j.tsep.2023.102382.
[19] D. Narducci, B. Lorenzi, Hybrid thermoelectric-photovoltaic solar harvesters: technological and economic issues, Jpn. J. Appl. Phys. 62 (2023), https://doi.org/10.35848/1347-4065/aca031. SD0801.
[20] https://gr.mouser.com/datasheet/2/433/WakefieldVette_Thermoelectic_Assemblies_TEMA_Data_-1874706.pdf.
[21] H. Najafi, K.A. Woodbury, Optimization of a cooling system based on Peltier effect for photovoltaic cells, Sol. Energy 91 (2013) 152–160, https://doi.org/10.1016/j.solener.2013.01.026.
[22] A. Gaur, G.N. Tiwari, Performance of photovoltaic modules of different solar cells, J. Sol. Energy. 2013 (2013) 1–13, https://doi.org/10.1155/2013/734581.
[23] J. Liu, Z. Zhao, J. Qian, Z. Liang, C. Wu, K. Wang, S. Liu, D. Yang, Thermal radiation annealing for overcoming processing temperature limitation of flexible perovskite solar cells, Adv. Mater. 36 (2024) 2401236, https://doi.org/10.1002/adma.202401236.
[24] W.G.J.H.M. van Sark, Feasibility of photovoltaic – thermoelectric hybrid modules, Appl. Energy 88 (2011) 2785–2790, https://doi.org/10.1016/j.apenergy.2011.02.008.
[25] S.B. Riffat, X. Ma, Thermoelectrics: a review of present and potential applications, Appl. Therm. Eng. 23 (2003) 913–935, https://doi.org/10.1016/S1359-4311(03)00012-7.
[26] https://www.ferrotec.com/products-technologies/thermoelectric-modules/.
[27] ABL Heatsinks website. http://www.abl-heatsinks.co.uk/, 2025.
[28] A.D. Jones, C.P. Underwood, A thermal model for photovoltaic systems, Fuel Energy Abstr 70 (2001) 349–389, https://doi.org/10.1016/S0140-6701(02)85831-3.
[29] J.H. Watmuff, W.W.S. Charters, D. Proctor, Solar and wind induced external coefficients - solar collectors, cooperation Mediterraneenne pour l'Energie Solaire, Revue Int. d'Heliotechn. 2nd Quarter (1977) 56.
[30] J.K. Kaldellis, M. Kapsali, K.A. Kavadias, Temperature and wind speed impact on the efficiency of PV installations. Experience obtained from outdoor measurements in Greece, Renew. Energy 66C (2014) 612–624, https://doi.org/10.1016/j.renene.2013.12.041.
[31] S. Misara, Thermal Impacts on Building Integrated Photovoltaic (BIPV), Electrical, Thermal and Mechanical Characteristics, 2014. Thesis.
[32] S.R. Raga, F. Fabregat-Santiago, Temperature effects in dye-sensitized solar cells, Phys. Chem. Chem. Phys. 15 (2013) 2328–2336, https://doi.org/10.1039/C2CP43220J.